Synthetic ferrimagnets with thermomagnetic switching

A. F. Kravets,[1,2,*] Yu. I. Dzhezherya,[1] A. I. Tovstolytkin,[1] I. M. Kozak,[1] A. Gryshchuk,[1] Yu. O. Savina,[3] V. A. Pashchenko,[3] S. L. Gnatchenko,[3] B. Koop,[2] and V. Korenivski[2]

[1]*Institute of Magnetism, National Academy of Sciences of Ukraine, 36 b Vernadsky Avenue, 03142 Kyiv, Ukraine*

[2]*Nanostructure Physics, Royal Institute of Technology, 10691 Stockholm, Sweden*

[3]*B. Verkin Institute for Low Temperature Physics and Engineering, National Academy of Sciences of Ukraine, 47 Lenin Avenue, 61103 Kharkiv, Ukraine*

(Received 11 June 2014; revised manuscript received 16 September 2014; published 29 September 2014)

Interlayer exchange coupling in strong/weak/strong ferromagnetic multilayers is investigated as a function of external magnetic field and temperature, with the focus on the magnetization switching near the Curie transition in the spacer composed of a diluted ferromagnet of concentration paramagnetic in the bulk. The effect of an externally applied reversing magnetic field on the width of the thermomagnetic transition is studied experimentally and explained theoretically as a result of the interplay between the proximity-induced exchange and the Zeeman effects in the system. Of high potential for applications should be the ability to switch one of the ferromagnetic outer layers using magnetic field, temperature, or a combination of the two.

DOI: 10.1103/PhysRevB.90.104427 PACS number(s): 75.20.En, 75.20.Hr, 75.30.Et, 75.70.Cn

I. INTRODUCTION

Interlayer exchange interactions in spin-valve-type magnetic multilayers, such as direct exchange [1], indirect oscillatory (RKKY) exchange [2–4], the magnetostatic Néel coupling [5–7], and exchange at ferromagnetic/antiferromagnetic interfaces [8,9], often dominate the magnetic ordering in the structure. These interactions are essentially fixed and cannot be affected by external parameters post-fabrication. The energy of these interactions is proportional to the strength of the magnetization in the ferromagnetic layers and for typical spin valves varies little for small changes in temperature near room temperature. It would be highly advantageous to be able to externally affect the strength of the intralayer and interlayer exchange interactions in a magnetic stack, as that could result in new types of devices based on magnetic switching via exchange coupling/decoupling of a suitable free layer.

Recently proposed [10,11] and experimentally demonstrated [12,13] is the effect of thermally controlled interlayer exchange coupling in trilayers of two strong ferromagnets (F) separated by a weakly ferromagnetic spacer (f), $F_1/f/F_2$ (so-called Curie valves), with a sharp thermomagnetic switching in the structure just above room temperature [14]. This switching was achieved by exchange decoupling of F_1 and F_2 when the weakly ferromagnetic spacer was thermally driven through its Curie point into the paramagnetic state.

Spacer f, determining the exchange between the outer layers F_1 and F_2, was diluted ferromagnetic alloy Ni_xCu_{100-x} [10–14]. Since Ni and Cu have fcc lattices with nearly equal lattice parameters ($a_{Ni} = 3.523$ Å, $a_{Cu} = 3.616$ Å), Ni_xCu_{100-x} alloys form at elevated temperatures up to 650 K single-phase fcc-lattice substitutional solid solutions (α phase), in which Ni and Cu are miscible in any proportions. At lower temperatures phase α dissociates into two, a Ni-rich phase α_1 and a Cu-rich phase α_2, yielding a two-phase solid-state solution [15]. Therefore, in bulk samples [16–18] as well as thin films of Ni_xCu_{100-x} deposited using magnetron sputtering [19], ferromagnetic clusters have been observed with magnetic moments of 8–12μ_B corresponding to ∼20–30 atoms of Ni and an average size of ∼5–10 nm.

The Curie temperature (T_C) of bulk [15] as well as film [20–23] samples of Ni_xCu_{100-x} alloys depends almost linearly on the Ni concentration. For x varying between ∼43–100 at.% the T_C monotonically increases from ∼0 K to 627 K. Thus, by selecting the magnetic dilution of the Ni-Cu spacer, and thereby its Curie point, one can regulate the temperature dependence of the exchange coupling in $F_1/f/F_2$ trilayer structures. The spacer is weakly ferromagnetic below its T_C^f and nominally paramagnetic above it. The proximity effect at the interface with a strong ferromagnet, however, can induce magnetization in a paramagnetic metal (F/P interface) [27,28], sometimes even in a nonmagnetic metal (F/N interface) [29,30]. This effect is typically accompanied by a reduction of the atomic magnetic moments in the strong ferromagnet at the interface [24–26] as well as by a substantial increase in the Curie point of the interfacial layer of the paramagnet [28]. It was recently observed [14] that in Curie valves of type $F_1/Ni_xCu_{100-x}/F_2$ the strength of the effective interlayer exchange coupling (F_1-F_2) varies nonlinearly with the thickness of the spacer, indicating a nonlinear distribution of the magnetization in the spacer, both below and above its Curie transition. Thus, the T_C of thin f(P) films enclosed by strongly ferromagnetic electrodes should be expected to significantly differ from that in the bulk. These proximity effects must be well understood, qualitatively and quantitatively, in order to develop useful magnetic nanodevices with thermomagnetic control.

Effective thermomagnetic control of the interlayer exchange coupling has recently been demonstrated [14] using a trilayer structure called a Curie switch (CS). The structure of CS is similar to that of a conventional spin valve [31,32], with the only difference being that the nonmagnetic metal spacer is replaced in CS with a layer of a diluted magnetic alloy, Ni_xCu_{100-x} in our case, in which the T_C is varied in fabrication by varying the Ni concentration in the alloy. The structure of such CS can be described as $F_1/f/F_{2\,pin}$, where F_1 is $Ni_{80}Fe_{20}$(10 nm); f, Ni_xCu_{100-x}(6 nm); $F_{2\,pin}$,

*Corresponding author: anatolii@kth.se

$Co_{90}Fe_{10}$(5 nm)/$Mn_{80}Ir_{20}$(12 nm); $x = 35$, 40, 45, and 52 at.% Ni. The magnetically soft permalloy layer, F_1, serves as the switching layer and the magnetically hard layer, $F_{2\,pin}$, exchange pinned to antiferromagnetic $Mn_{80}Ir_{20}$ serves as the reference layer of the spin valve. The type of the antiferromagnet (Mn-Ir) and its thickness of 12 nm were chosen for increased thermal stability and large magnitude of the exchange pinning of $F_{2\,pin}$, $Co_{90}Fe_{10}$ [33]. The magnetization in layers F_1 and $F_{2\,pin}$ in the F_1/f/$F_{2\,pin}$ structure, when weakly exchange coupled, can rotate in response to an external magnetic field independently. Therefore, one of the states of the trilayer is where F_1 and $F_{2\,pin}$ are magnetized in opposition, such that the net magnetic moment of the structure is nearly zero. The above Curie switching is similar in spirit but is different in mechanism from the thermally assisted switching reported in Ref. [34].

The thickness of the $Ni_{80}Fe_{20}$ (10 nm) and $Co_{90}Fe_{10}$ (5 nm) layers was chosen such that the layers had approximately equal magnetic moments, and the thickness of the Ni_xCu_{100-x} spacer (6 nm) was chosen to avoid any indirect exchange (RKKY) or magnetostatic (Néel) coupling. RKKY in Ni_xCu_{100-x} spacers vanishes for thicknesses above ~5 nm [35–39], similarly to the behavior in conventional spin valves with nonmagnetic Cu spacers, where RKKY goes to essentially zero over ~5 nm [40]. The Néel coupling, which can be responsible in particular for offsetting the minor loop of the switching layer in spin-valves, also vanishes with increasing spacer thickness and becomes insignificant at above ~5 nm [7,41].

In this work, we investigate, in a wide temperature range, the magnetic phase space of the Curie switch, the switching in which is determined by the interplay of the F_1-F_2 exchange coupling across the weakly ferromagnetic/paramagnetic spacer f and the Zeeman energy of the soft ferromagnetic layer F_1 in an external magnetic field. The former is a nontrivial function of temperature due to the overlap of the intrinsic Curie transition and the interface-induced proximity effects in the spacer. We develop a detailed theoretical model of the system, and obtain an analytical expression for the effective switching field and its functional form versus temperature. The model takes into account the significantly nonlinear profile of the exchange and local magnetization throughout the thickness of the switch. The result is that magnetic switching can be achieved by either a temperature or field sweep, or a combination of the two where the sensitivity of the magnetic transition to external field and temperature are interdependent parameters. We fully confirm the analytical result using a micromagnetic simulation.

II. PHENOMENOLOGY OF CURIE SWITCHING

The thermomagnetic effects in the F_1/f/$F_{2\,pin}$ structure (Fig. 1) are described using a phenomenological model, in which the two ferromagnetic interfaces F_1/f and f/$F_{2\,pin}$ are strongly coupled by the exchange interaction, primarily due to the conduction electrons in the respective metals. This exchange leads to enhanced magnetism in the interfacial layers of the diluted ferromagnet f. It is then natural to assume that the magnitude of the spacer magnetization reaches its maximum at the interface, m_0, and its direction coincides with the direction of the magnetization in F_1 and $F_{2\,pin}$. The free energy of the

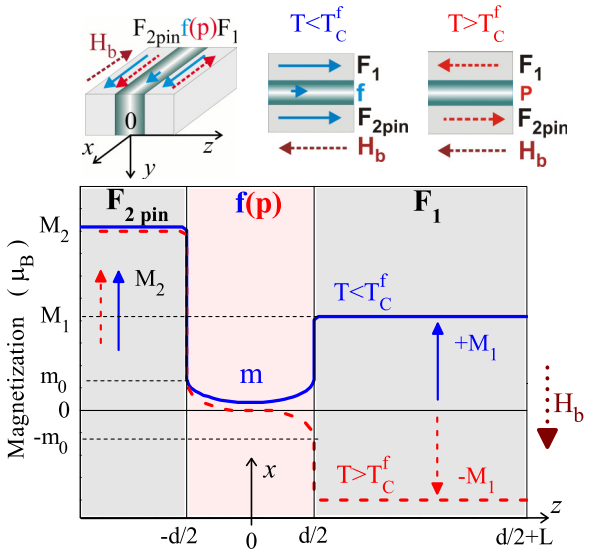

FIG. 1. (Color online) Magnetization distribution in F_1/f/$F_{2\,pin}$ Curie switch at high ($T > T_C^f$) and low ($T < T_C^f$) temperatures. The upper panel illustrates the configuration of the magnetic moments M_1 and M_2 of the layers at below and above the Curie temperature; the arrows indicate the direction of the magnetic moments of the layers.

structure F_1/f/$F_{2\,pin}$ becomes

$$F = \int_{-d/2}^{d/2} \left[\frac{\alpha}{2} \left(\frac{d\mathbf{m}}{dz} \right)^2 + m_x H + f(m) + \frac{\mathbf{H}_m^2}{8\pi} \right] dz + 2\sigma + M_{1x} H L. \quad (1)$$

Axis Oz in (1) is taken to point perpendicularly to the film plane and external magnetic field $\mathbf{H}$ along the Ox axis, opposite to the equilibrium (all parallel) magnetization of the trilayer. The first term, in the form of an integral, describes the magnetic energy of the diluted ferromagnetic spacer f, and includes the exchange contribution (α, the exchange constant), the Zeeman contribution, and a phenomenological term $f(m)$ which depends on the magnitude of the effective magnetization in the structure. The term containing $\mathbf{H}_m$ takes into account the magnetostatic energy of the system. The term 2σ describes the interaction of the spacer with the ferromagnetic outer layers at the two interfaces, F_1/f and f/$F_{2\,pin}$, and is a constant since here the spacer spins are saturated in the direction of F_1 and $F_{2\,pin}$. Finally, the last term in (1) describes the Zeeman effect of the external field on the switching layer, F_1. Here M_{1x} is the magnetization of the switching layer and L its thickness.

For determining the functional form of $f(m)$, we use the results of the Stoner theory [42], representing it in the form of a series in even powers of the magnetization:

$$f(m) = \frac{m^2}{2\chi} + \frac{gm^4}{4} + \cdots, \quad (2)$$

where, in accordance with the Curie-Weiss law, $\chi = C/(T - T_C^f)$ is the magnetic susceptibility of the spacer's material, T_C^f is its Curie temperature, and g is the expansion coefficient. Here and in what follows we take $T > T_C^f$, corresponding to the case of low Ni concentration, in focus in this work, with the intrinsic state of the spacer being paramagnetic. Any magnetic polarization of the spacer is then solely due to the influence

of the surrounding ferromagnetic layers. In the paramagnetic state $1/\chi \gg 1$, and m is a small value, so that in Eq. (2) it is sufficient to consider the first term of the expansion. A similar approach has successfully been used in the description of the temperature dependence of the interface exchange coupling in a system of Co nanocrystals highly diluted in an amorphous matrix [43].

Taking into account the uniformity of the structure in the plane of the multilayer, the magnetization distribution depends on one coordinate only, z, perpendicular to the film plane. The Maxwell equation $\mathrm{div}\mathbf{B} = 0 \Rightarrow \frac{\partial}{\partial z}(H_m^z + 4\pi m_z) = 0$ therefore yields $\mathbf{H}_m = -4\pi m_z \mathbf{e}_z$. It is then convenient to represent the spacer magnetization in terms of the angular variables: $\mathbf{m} = m(\cos\varphi \sin\theta, \sin\varphi \sin\theta, \cos\theta)$, where θ,φ are the polar and azimuthal angles of the $\mathbf{m}$ vector, with the polar axis being Oz.

Using the above notations, the free energy of the system takes the form

$$F = \frac{1}{2}\int_{-d/2}^{d/2} dz \left\{ \alpha \left(\frac{dm}{dz}\right)^2 + \alpha m^2 \left[\left(\frac{d\theta}{dz}\right)^2 + \sin^2\theta \left(\frac{d\varphi}{dz}\right)^2 \right] + 2mH\cos\varphi\sin\theta + \frac{m^2}{\chi} + 4\pi m^2 \cos^2\theta \right\} + M_1 \cos\varphi_0 H L + 2\sigma. \quad (3)$$

Other notations implicit in (3) are that the magnetization $\mathbf{M}_2$ of the pinned layer $F_{2\,\mathrm{pin}}$ is oriented along Ox, and angle φ_0 describes the deviation of $\mathbf{M}_1$ from Ox, which also is the direction of the external magnetic field. Thus, φ_0 defines the change in the system energy on rotation of the switching layer F_1 with respect to the pinned layer $F_{2\,\mathrm{pin}}$.

A. Variational equation for magnetization vector

The variational problem of finding the energy minimum of the system with respect to the magnetization parameters m,θ,φ results in the following equations (4a), (4b), and (4c) and boundary conditions at the interfaces (4d):

$$-\frac{d^2m}{d\xi^2} + \left[\left(\frac{d\theta}{d\xi}\right)^2 + \sin^2\theta \left(\frac{d\varphi}{d\xi}\right)^2 + 4\pi\chi\cos^2\theta \right] m + m + \chi H \cos\varphi \sin\theta = 0, \quad (4a)$$

$$-\frac{d}{d\xi}\left(m^2 \frac{d\theta}{d\xi}\right) + m^2 \left[\left(\frac{d\varphi}{d\xi}\right)^2 - 4\pi\chi \right] \sin\theta\cos\theta + \chi H m \cos\varphi\cos\theta = 0, \quad (4b)$$

$$\frac{d}{d\xi}\left(m^2 \sin^2\theta \frac{d\varphi}{d\xi}\right) + \chi H m \sin\varphi \sin\theta = 0, \quad (4c)$$

$$m(\pm d/2) = m_0, \quad \theta(\pm d/2) = \pi/2, \quad \varphi(-d/2) = 0, \quad \varphi(d/2) = \varphi_0. \quad (4d)$$

Introduced here is a new notation $\xi = z/\lambda$, $\lambda = \sqrt{\alpha\chi}$, which is the characteristic length scale in the problem.

Analyzing the above boundary-value problem (4a)–(4d) yields $\theta(\xi) = \pi/2$, which significantly simplifies the system of equations:

$$-\frac{d^2m}{d\xi^2} + \left(\frac{d\varphi}{d\xi}\right)^2 m + m = -\chi H \cos\varphi, \quad (5a)$$

$$\frac{d}{d\xi}\left(m^2 \frac{d\varphi}{d\xi}\right) = -\chi H m \sin\varphi. \quad (5b)$$

Further simplification is due to the fact that for a material in the paramagnetic state the following condition holds: $\chi H \ll m_0$. Therefore, neglecting the right-hand side of Eqs. (5), we arrive at

$$\frac{d\varphi}{d\xi} = B\frac{m_0^2}{m^2}, \quad \varphi(\xi) = B\int_{-d/2\lambda}^{\xi} d\eta \frac{m_0^2}{m(\eta)^2}, \quad -\frac{d^2m}{d\xi^2} + m + B^2\frac{m_0^4}{m^3} = 0, \quad (6)$$

where B is the constant of integration depending on the boundary conditions (4).

The system of equations (6) is integrated in elementary functions and, subject to conditions (4d), yields the following spatial variations:

$$m(\xi) = \frac{m_0}{\sinh(d/\lambda)} \times \sqrt{\cosh 2\xi - 1 + \cos\varphi_0[\cosh(d/\lambda) - \cosh 2\xi]}, \quad (7a)$$

$$\tan\varphi = \tan(\varphi_0/2)\frac{\tanh(d/2\lambda) + \tanh(\xi)}{\tanh(d/2\lambda) - \tanh(\xi)\tan^2(\varphi_0/2)}. \quad (7b)$$

It follows from (7) that for the parallel ordering of the magnetic moments of layers F_1 and F_2, $\varphi = 0$, $m(\xi) = m_0\cosh\xi/\cosh(d/2\lambda)$, while for the antiparallel ordering, $\varphi = \pi$, $m(\xi) = m_0\sinh\xi/\sinh(d/2\lambda)$.

Figure 2 shows the calculated spatial dependence of the magnetization in the spacer f of a F_1/f/$F_{2\,\mathrm{pin}}$ Curie switch for parallel ($\varphi = 0$) and antiparallel ordering of the magnetic moments of the outer layers ($\varphi = \pi$).

Despite the fact that the distribution of the magnetization (7) was found for arbitrary angles, when analyzing the stability of the system we can consider energy changes for small deviations of the magnetization of the ferromagnetic layers F_1 and F_2 from parallel orientation.

Then, assuming $\varphi_0 \ll 1$, and taking into account the boundary conditions (4d), we find the solution to (6) for the

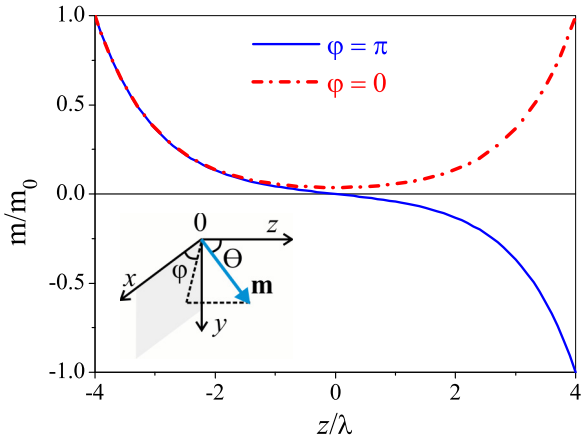

FIG. 2. (Color online) Theoretical magnetization distribution in the spacer (f) of a F_1/f/$F_{2\,pin}$ Curie switch for parallel ($\varphi = 0$) and antiparallel ordering of the magnetic moments of the outer layers ($\varphi = \pi$). The temperature in this illustration is chosen such that the interlayer exchange from the induced ferromagnetism is "pinched off" in the center of the spacer.

modulus of the magnetization vector, accurate to the terms proportional to φ_0^2:

$$m(\xi) = \frac{m_0 \cosh(\xi)}{\cosh(d/2\lambda)} - \frac{m_0\varphi_0^2}{8\sinh^2(d/2\lambda)} \times \left[\frac{\cosh(d/2\lambda)}{\cosh(\xi)} - \frac{\cosh(\xi)}{\cosh(d/2\lambda)}\right], \tag{8a}$$

$$\varphi(\xi) = \frac{\varphi_0}{2}\left[1 + \frac{\tanh(\xi)}{\tanh(d/2\lambda)}\right]. \tag{8b}$$

It follows from (8) that for $d/\lambda \leqslant 1$ the magnetization at the interface is essentially independent from temperature and close to its maximum value m_0, due to the exchange interaction with the strong ferromagnets F_1 and $F_{2\,pin}$. In the opposite limiting case, $d/\lambda \gg 1$, the magnetization in the center of the spacer vanishes exponentially.

B. Equilibrium state of Curie switch

After finding the magnetization distribution in the spacer f of F_1/f/$F_{2\,pin}$, we proceed to find the energy of the exchange interaction between the ferromagnetic layers F_1 and $F_{2\,pin}$ (indirect, via the spacer) and, specifically, the temperature dependence of the effective exchange constant.

From (3), accurate to second order in small φ_0, we find

$$F = F_0 + J\varphi_0^2/2,$$
$$F_0 = \lambda\left(m_0^2/2 + Hm_0\right)\tanh(d/2\lambda) + M_1 HL + 2\sigma, \tag{9}$$
$$J = \frac{m_0^2\lambda}{\chi\sinh(d/\lambda)} - H\left(M_1 L + \frac{m_0\lambda}{2}\tanh(d/2\lambda)\right).$$

Coefficient J in Eq. (9) essentially is the exchange integral between the ferromagnetic layers F_1 and $F_{2\,pin}$. The positive contribution to J decreases exponentially with the increase of the spacer thickness.

For positive J, small deviations of the soft layer magnetization M_1 lead to an increase of the energy. In this case the system maintains stability in an external magnetic field applied opposite to the ferromagnetic layers' magnetization.

Thus, the criterium of stability of the Curie switch in a magnetic field has the form

$$H < \frac{\lambda m_0^2}{\chi\sinh(d/\lambda)[M_1 L + (\lambda m_0/2)\tanh(d/2\lambda)]}. \tag{10}$$

Since the spacer material is a diluted ferromagnet, and condition $2M_1 L \gg m_0\lambda$ holds, Eq. (10) simplifies to

$$HM_1 < \frac{1}{\chi}\frac{\lambda}{L}\frac{m_0^2}{\sinh(d/\lambda)}. \tag{11}$$

It follows from (11) that the critical magnetic field necessary for reorienting the soft ferromagnetic layer is a strong function of temperature. Using the standard temperature dependence of the magnetic susceptibility, $\chi = C/(T - T_C^f)$, the explicit form of the temperature dependence becomes

$$HM_1 = \frac{m_0^2}{L}\frac{\sqrt{\alpha\left(T - T_C^f\right)/C}}{\sinh\left(d\sqrt{\left(T - T_C^f\right)/\alpha C}\right)}. \tag{12}$$

The Curie constant C can be estimated as follows: $C = xC_{Ni}$, where C_{Ni} is the Curie constant for pure Ni (above T_C^f) and x is Ni atomic content in the spacer material, Ni_xCu_{1-x}. For estimates in the vicinity of room temperature, it is convenient to rewrite (12) as

$$H = \frac{\delta}{L}\frac{m_0^2}{\chi_0 M_1}\frac{\sqrt{\left(T - T_C^f\right)/T_0}}{\sinh\left(\frac{d}{\delta}\sqrt{\left(T - T_C^f\right)/T_0}\right)}, \tag{13}$$

where T_0 is room temperature, $\chi_0 = C/T_0 \sim 10^{-2}$–$10^{-4}$ is magnetic susceptibility of the spacer material, and $\delta = \sqrt{\alpha C/T_0}$ is the characteristic length scale of the system.

III. EXPERIMENTAL METHODS

Magnetic multilayers $Ni_{80}Fe_{20}$(10 nm)/Ni_xCu_{100-x}(6 nm)/$Co_{90}Fe_{10}$(5 nm)/$Mn_{80}Ir_{20}$(12 nm), where $x = 35$, 40, 45, 52 at.% Ni (in what follows F_1/Ni_xCu_{100-x}/$F_{2\,pin}$) were deposited at room temperature on thermally oxidized silicon substrates using magnetron sputtering in an AJA Orion 8-target system. The base pressure in the chamber was $\sim 6\times10^{-9}$ Torr. The sputtering gas was Ar at 5 mTorr pressure. The substrates were rotated at 32 rpm during depositions. The ferromagnetic layers $Ni_{80}Fe_{20}$ (F_1) and $Co_{90}Fe_{10}$ ($F_{2\,pin}$), as well as antiferromagnetic $Mn_{80}Ir_{20}$ (AFM), were sputtered from single targets. The diluted ferromagnetic spacer Ni_xCu_{100-x} with $x = 35$, 40, 45, and 52 at.% was deposited by co-sputtering from pure Cu and Ni targets. The composition of the Ni_xCu_{100-x} spacer was regulated by selecting suitable rates of deposition of Ni and Cu, r_{Ni} and r_{Cu}, controlled using a quartz thickness monitor. In this the relation between the thickness monitor weights, y, and the expected atomic fractions, x, in the Ni_xCu_{100-x} alloy was taken into account according to $x = 100y/[y + (100 - y)m_{Ni}/m_{Cu}]$, where m_{Ni} and m_{Cu} are Ni and Cu atomic weights, respectively. Weight concentrations y in Ni_yCu_{100-y} are related with r_{Ni} and r_{Cu} as $y/(100 - y) = (\rho_{Ni}/\rho_{Cu})(r_{Ni}/r_{Cu})$, where ρ_{Ni} and ρ_{Cu} are

the densities of Ni and Cu, respectively. Thus calculated and maintained during deposition of the spacer rates of Ni, r_{Ni}, and Cu, r_{Cu}, for $x = 35$, 40, 45, and 52 at.% Ni were, respectively, 0.0339 and 0.068; 0.0339 and 0.055; 0.0527 and 0.0697; 0.0717 and 0.0722 nm/sec.

The exchange pinning between the ferromagnetic $Co_{90}Fe_{10}$ and antiferromagnetic $Mn_{80}Ir_{20}$ was set in during deposition of the multilayer using an in-plane magnetic field $H_{dep} \approx 1$ kOe. The magnetization measurements as a function of magnetic field and temperature were performed using a SQUID magnetometer MPMS-XL5 Quantum Design, in the temperature range of 5–400 K, and in magnetic fields of up to 5 kOe applied in the film plane and parallel to the pinning direction of H_{dep}.

IV. RESULTS AND DISCUSSION

Figure 3 shows the magnetization loops of $F_1/Ni_xCu_{100-x}/F_{2\,pin}$ with $x = 35$, 40, 45, and 52 at.% Ni, measured at $T = 300$ K and $T = 5$ K, for multilayer samples of 3.5×3.5 mm^2 in-plane dimensions. The loops consist of two parts, minor and major, corresponding respectively to switching of the soft F_1 and pinned layer $F_{2\,pin}$.

The pinned layer $F_{2\,pin}$ is reversed far from zero field due to the exchange coupling to the antiferromagnet. The soft layer F_1, for low Ni concentrations in the spacer ($x = 35$ and 40 at.%, paramagnetic in the bulk) should ideally switch near zero field. Experimentally, however, a nonzero loop offset is present, H_{coupl}, which must be due to the spacer-mediated interaction with the pinned ferromagnetic layer. The overall form of the magnetization loops of the CS is similar to that for conventional spin valves (SVs) [31,32], with the difference being the offset of the minor loop, typically zero for SVs with 6 nm thick spacers (zero interlayer exchange and vanishing Néel coupling [41]) while in the CS the offset H_{coupl} can be significant and strongly depends on temperature due to the Curie transition in the spacer, acting as an on/off switch for the interlayer exchange coupling between F_1 and $F_{2\,pin}$. The data in Fig. 3 shows that F_1, especially at low temperature, reverses gradually rather than switches sharply. This indicates that even for these nominally paramagnetic concentrations of the spacer (in the bulk) the proximity of the interfaces mediates nonzero exchange through the spacer.

In the intermediate plateau range (approximately -100 to -400 Oe) in Fig. 3(a), where the net magnetization is nearly zero, the magnetic moments of the strongly ferromagnetic layers F_1 and $F_{2\,pin}$ align antiparallel to each other.

The magnetization loops show the characteristic exchange fields, H_{coupl} and H_{eb} [see Fig. 3(d)], where H_{coupl} is the field corresponding to the exchange coupling between F_1 and $F_{2\,pin}$, and H_{eb} is the field of exchange pinning between F_2 and AFM. As x increases, both for $T = 300$ K and $T = 5$ K, the effective magnetization in the spacer increases, which enhances the interlayer exchange. The effect is an increase in the magnitude of H_{coupl} and and a decrease in H_{eb}, which eventually merge in one transition [Fig. 3(d), for $T = 5$ K].

The difference between the two exchange fields can be used as the quantity characterizing the strength interlayer exchange between F_1 and $F_{2\,pin}$ through the Ni_xCu_{100-x} spacer, for

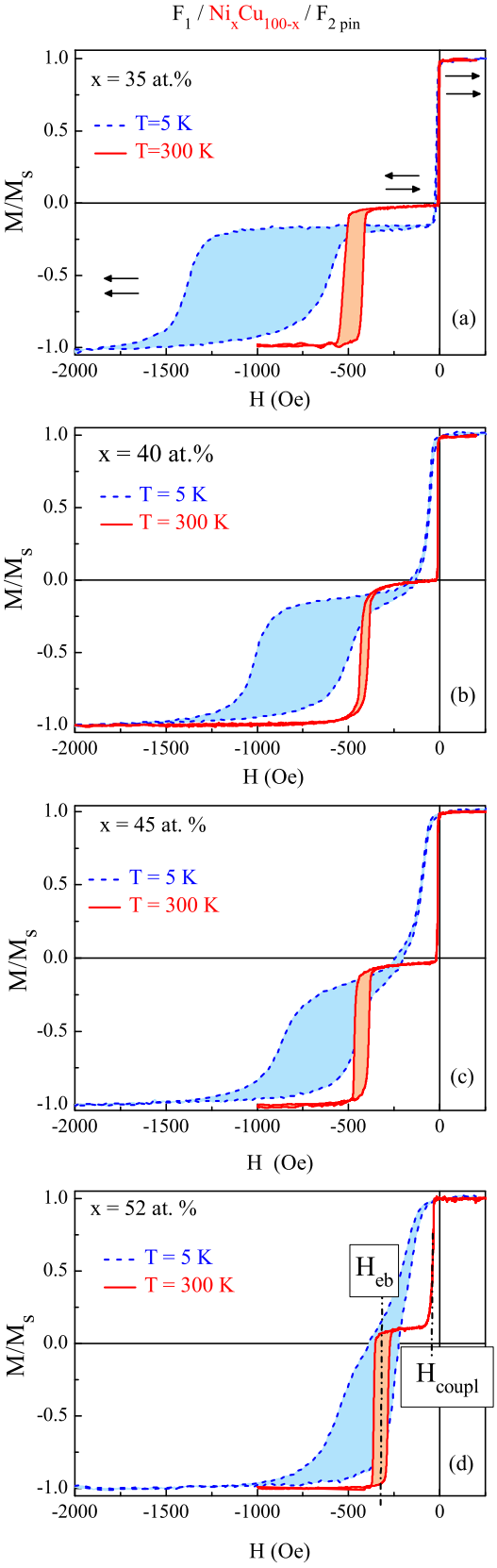

FIG. 3. (Color online) Magnetization loops of $F_1/Ni_xCu_{100-x}/F_{2\,pin}$, measured at $T = 300$ K and $T = 5$ K. (a) $x = 35$ at.% Ni; (b) $x = 40$ at.% Ni; (c) $x = 45$ at.% Ni; (d) $x = 52$ at.% Ni.

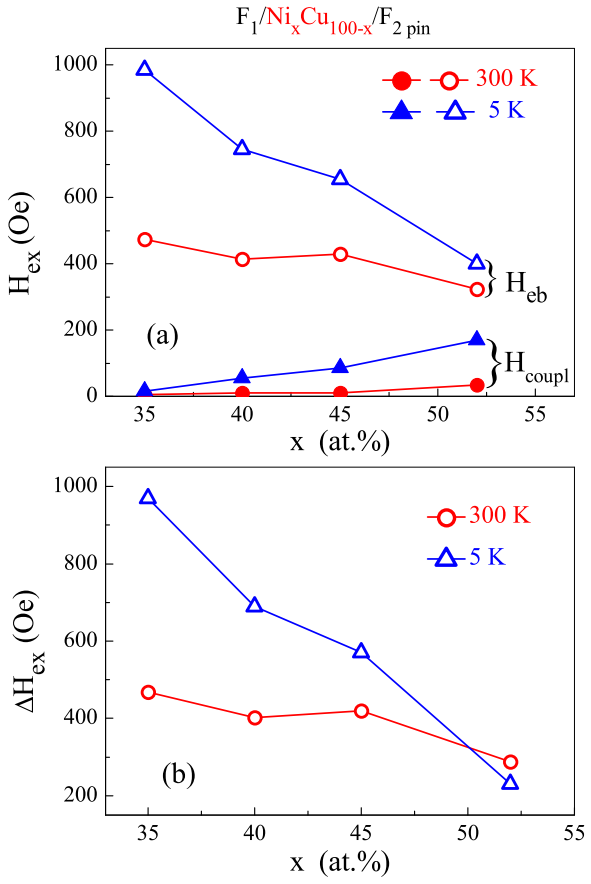

FIG. 4. (Color online) (a) Exchange fields H_{coupl} and H_{eb} and (b) their difference ΔH_{ex} for $F_1/Ni_xCu_{100-x}/F_{2\,pin}$ with $x = 35$, 40, 45, and 52 at.% Ni, measured at $T = 300$ K and $T = 5$ K.

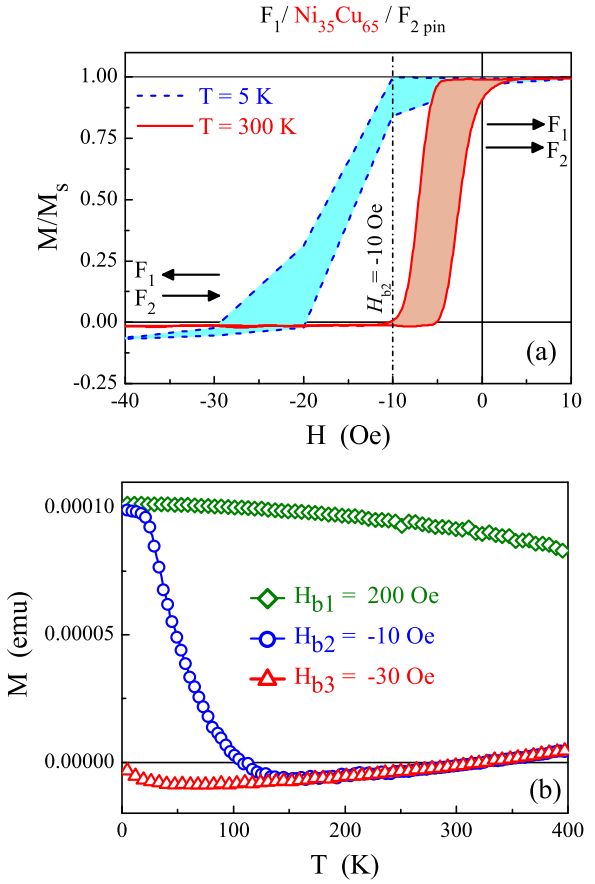

FIG. 5. (Color online) (a) Magnetization minor loops and (b) its temperature dependence for $F_1/Ni_{35}Cu_{65}/F_{2\,pin}$ measured in three characteristic applied fields H_b.

given temperature and concentration: $\Delta H_{ex} = H_{eb} - H_{coupl}$ [Fig. 4(b)]. The smaller the ΔH_{ex}, the stronger the interlayer exchange interaction. Figure 4(b) shows that at $T = 5$ K the interlayer exchange strength monotonically increases (ΔH_{ex} decreases) as the Ni concentration in the spacer increases.

Figures 5(a) and 5(b) show the minor loops for $F_1/Ni_{35}Cu_{65}/F_{2\,pin}$ measured at $T = 5$ K and $T = 300$ K, and the temperature dependence of the magnetization recorded at three characteristic applied fields. We note that the alloy of this composition, $Ni_{35}Cu_{65}$ (as well as $Ni_{40}Cu_{60}$) is paramagnetic at all temperatures in the bulk [15] and single-film form [20–22]. The data of Fig. 5 show that the proximity of strongly ferromagnetic interfaces induces nonzero ferromagnetic order in the spacer material across at least 6 nm of its thickness. The effective Curie temperatures of $Ni_{35}Cu_{65}$ and $Ni_{40}Cu_{60}$ are thereby significantly increased. As a result, the proximity-induced magnetic order mediates the exchange between the two spacers' interfaces at F_1 and $F_{2\,pin}$ in $F_1/Ni_{35}Cu_{65}/F_{2\,pin}$ and $F_1/Ni_{40}Cu_{60}/F_{2\,pin}$, which become exchange coupled even at room temperature. A similar in nature noticeable enhancement of the Curie temperature of the amorphous matrix in Fe-B-Nb-Cu nanocrystalline alloys, mainly due to magnetic interaction with the Fe particles having higher Curie temperature, has been reported by Hernando *et al.* [44]. This enhancement was explained by penetration of the exchange field of the Fe nanocrystals into the amorphous paramagnetic intergranular regions.

Increasing the temperature above the effective Curie point (T_C^f) of the diluted spacer $Ni_{35}Cu_{65}$ subject to a weak reversing magnetic field H_b (−10 Oe) leads to magnetization switching of F_1 in $F_1/Ni_{35}Cu_{65}/F_{2\,pin}$, from parallel to antiparallel alignment with respect to the pinned layer $F_{2\,pin}$. Since the magnetic moments of F_1 and $F_{2\,pin}$ are equal in magnitude, the net magnetic moment of the structure becomes zero. Such switching, in view of its thermomagnetic character, was termed Curie switching (CS) [14].

Figure 6 shows the magnetic properties of the $F_1/Ni_{40}Cu_{60}/F_{2\,pin}$ trilayer. The minor magnetization loops are shown in Fig. 6(a) for $T = 5$ K and $T = 300$ K. The dashed lines show the reversing fields H_b applied to the structure during the temperature sweeps shown in Fig. 6(b). The data clearly show that the position T_{tr} and sharpness dT_{tr} of the magnetic transition in temperature strongly depend on the applied magnetic field H_b. These transition characteristics, T_{tr} and dT_{tr}, were obtained by differentiating the measured $M(T)$, which are shown in Fig. 6(c), and Gaussian-interpolating the result. The obtained T_{tr} and dT_{tr} are shown in Fig. 6(d). T_{tr} increases and dT_{tr} decreases for lower applied fields H_b. Similar behavior is observed for other concentrations x. Thus, by varying H_b one can vary the temperature and width of the Curie switching in the synthetic ferrimagnetic structure, $F_1/f/F_{2\,pin}$. The thermomagnetic effect is very strong—a

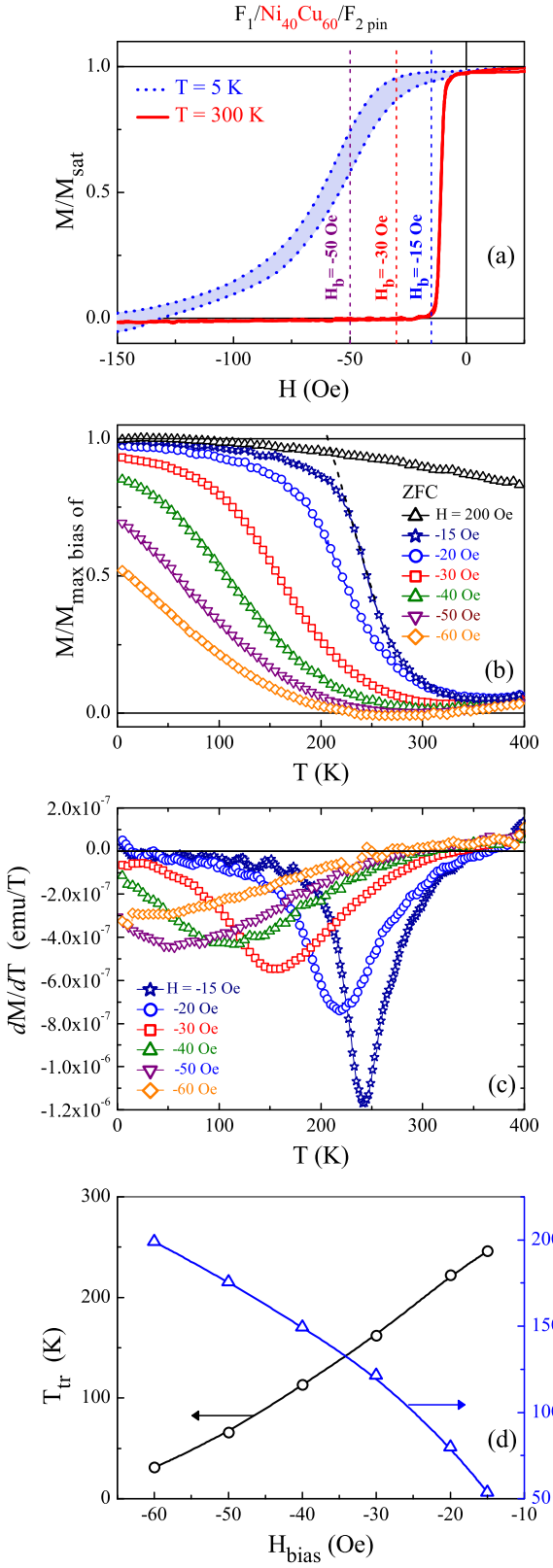

FIG. 6. (Color online) Magnetic properties of $F_1/Ni_{40}Cu_{60}/F_{2\,pin}$ Curie switch. (a) Minor magnetization loops for $T = 5$ K and $T = 300$ K. The dashed lines show the characteristic biasing fields H_b used in (b)–(d). (b) Magnetization versus temperature measured in various H_b. (c) First derivative of $M(T)$ curves shown in (b). (d) Position T_{tr} and half width dT_{tr} of the Curie switching shown in (c).

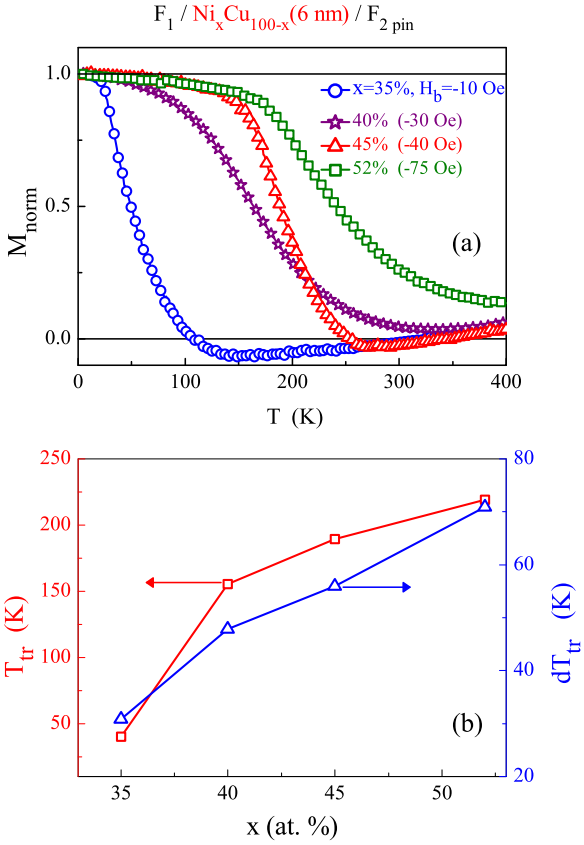

FIG. 7. (Color online) (a) Magnetization versus temperature measured in optimal biasing fields; (b) temperature T_{tr} and half width dT_{tr} of the Curie transition for trilayers $F_1/Ni_xCu_{100-x}/F_{2\,pin}$ with $x = 35$, 40, 45, and 52 at.% Ni.

change in H_b of a few tens of Oe results in changes of T_{tr} of hundreds of K.

Figure 7(a) shows the M-T transitions for four spacer concentrations measured under optimum biasing (corresponding to narrowest transition for each x). T_{tr} and dT_{tr} extracted as described above for $F_1/Ni_xCu_{100-x}/F_{2\,pin}$ with $x = 35$, 40, 45, and 52 at.% Ni are shown in Fig. 7(b). The data show that for increasing x, the stronger proximity effect in the spacer increases the Curie-transition temperature and its width.

Figure 8 shows the measured temperature dependence of the switching field in a CS, fitted using the the analytical result of (13). Experimentally, the switching temperature for a given applied field was determined as the point of intersection of the tangent to the M-T transition with the horizontal line [with the saturation magnetization line, as shown in Fig. 6(b)]. The agreement between the experiment and theory is very good, for reasonable sample parameters. This supports our interpretation of the mechanisms involved and offers a practical formula for designing or optimizing relevant thermomagnetic heterostructures and devices.

V. MICROMAGNETIC SIMULATION OF MAGNETIZATION PROFILE IN SPACER

We next simulate the switching in the Curie switch micromagnetically, using OOMMF with the theta evolve module,

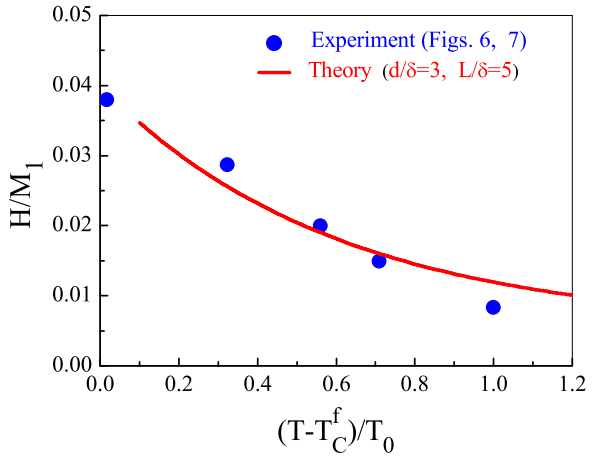

FIG. 8. (Color online) Measured temperature dependence of the switching field in $Ni_{80}Fe_{20}$(10 nm)/$Ni_{40}Cu_{60}$(6 nm)/$Co_{90}Fe_{10}$(5 nm)/$Mn_{80}Ir_{20}$(12 nm), fitted using the analytical result (13) with the following parameters: $\chi_0 = C/T_0 = 0.016$, $m_0/M_1 = 0.1$, $d/\delta = 3$, and $L/\delta = 5$.

which models finite temperatures via a differential equation of the Langevin type [45]. The simulation results are shown in Fig. 9.

In a typical simulation, the magnetization throughout the spacer (f) reached its equilibrium in approximately 250 ps. The total simulation time was 500 ps. The plots shown in Fig. 9 consist of the average magnetization over each cell layer over the last 125 ps of the simulation. The simulation data were fitted with the theoretical prediction for the magnetization profile in the spacer using m_0 and temperature as the fitting parameters. The temperatures shown in Fig. 9 are the temperatures used in the simulation. In order to keep the simulation time within reasonable bounds, only the magnetization of the spacer f was simulated and ferromagnetic outer layers were modeled via boundary conditions as full magnitude, parallel and antiparallel interface-spin orientation. This has shown to be a good approximation since the T_C of the F_1 and F_2 layers is much higher than that of the spacer f. It was important to use a small cell size, in our case 5×5×5 Å, and a rather short time step of 10^{-16} s to have a realistic thermal agitation. A full quantitative agreement should not be expected as with the atomistic spin-dynamic codes [46]; nevertheless, we obtain an excellent qualitative agreement with the analytical theory presented above and are able to clearly visualize the thermomagnetic switching process in the system—a Bloch wall type exchange spring in the proximity-ferromagnetic spacer at low temperature, pinched off in the middle of the spacer by a rise in the temperature.

VI. CONCLUSION

We develop a theoretical model of the thermomagnetic switching in a Curie switch, and obtain analytical expressions for the effective switching field and its functional form versus temperature. The model takes into account the significantly nonlinear profile of the exchange and local magnetization throughout the thickness of the switch, and specifically in the

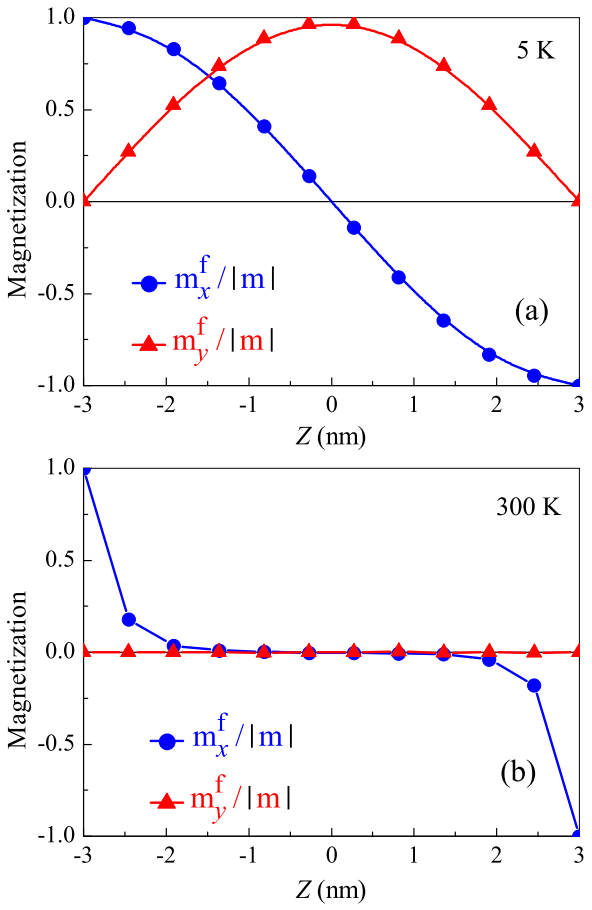

FIG. 9. (Color online) (a) The two components of the spacer magnetization at low temperature of 5 K, with the outer layers F_1 and F_2 set in to the antiparallel alignment. The component along the easy axis, m_x (direction of the exchange pinning), has the structure of Bloch wall type, with the spins rotating in the film plane. The perpendicular in-plane component, m_y, is maximum in the center of the spacer ($z = 0$). Solid lines show the fits using the analytical theory. (b) As the temperature is increased well above the T_C^f of the spacer (here to 300 K), the spacer becomes paramagnetic in the middle, m_y becomes zero everywhere in f, and m_x rapidly decays away from the interfaces and is always along the easy axis.

spacer where proximity-induced magnetism plays the key role. The result is that magnetic switching can be achieved by either a temperature or field sweep, or a combination of the two where the sensitivity of the magnetic transition to external field and temperature are interdependent parameters. A micromagnetic simulation details the thermomagnetic transition in the spacer as a Bloch wall type exchange spring versus the interface-induced ferromagnetic skin effect.

We experimentally demonstrate thermomagnetic control of the interlayer exchange coupling in synthetic ferrimagnets of type F_1/f/$F_{2\,pin}$, with F_1 being $Ni_{80}Fe_{20}$(10 nm); f, Ni_xCu_{100-x} (6 nm); $F_{2\,pin}$, $Co_{90}Fe_{10}$(5 nm)/$Mn_{80}Ir_{20}$ (12 nm); $x = 35$, 40, 45, and 52 at.% Ni. The observed thermomagnetic effect is very strong—a change in the biasing field of only a few tens of Oe results in changes of the transition temperature of hundreds of K. This offers a way of magnetization control in nanoscale magnetic devices.

ACKNOWLEDGMENTS

This work was supported by the Targeted Comprehensive Fundamental Research Program of the National Academy of Science of Ukraine under the program "Fundamental Problems of Nanostructured Systems, Nanomaterials, and Nanotechnologies", Project No. 22/14-H, and the Swedish Foundation Olle Engkvist Byggmästare under the grant "Spin-Thermo-Electronics".

[1] M. H. Bozorth, *Ferromagnetism* (D. Van Nostrand Company, Inc., Princeton, 1951).
[2] S. S. P. Parkin, N. More, and K. P. Roche, Phys. Rev. Lett. **64**, 2304 (1990).
[3] S. S. P. Parkin, Phys. Rev. Lett. **67**, 3598 (1991).
[4] P. Bruno and C. Chappert, Phys. Rev. Lett. **67**, 1602 (1991).
[5] L. Néel, C. R. Hebd. Seances Acad. Sci., Ser. A **255**, 1545 (1962); **255**, 1676 (1962).
[6] J. C. Bruyère, G. Clerc, O. Massenet, R. Montmory, L. Néel, D. Paccard, and A. Yelon, J. Appl. Phys. **36**, 944 (1965).
[7] T. C. Schulthess and W. H. Butler, J. Appl. Phys. **87**, 5759 (2000).
[8] W. H. Meiklejohn and C. P. Bean, Phys. Rev. **102**, 1413 (1956).
[9] W. H. Meiklejohn and C. P. Bean, Phys. Rev. **105**, 904 (1957).
[10] A. M. Kadigrobov, S. Andersson, D. Radić, R. I. Shekhter, M. Jonson, and V. Korenivski, J. Appl. Phys. **107**, 123706 (2010).
[11] A. M. Kadigrobov, S. Andersson, Hee Chul Park, D. Radić, R. I. Shekhter, M. Jonson, and V. Korenivski, J. Appl. Phys. **111**, 044315 (2012).
[12] S. Andersson and V. Korenivski, J. Appl. Phys. **107**, 09D711 (2010).
[13] S. Andersson and V. Korenivski, IEEE Trans. Magn. **46**, 2140 (2010).
[14] A. F. Kravets, A. N. Timoshevskii, B. Z. Yanchitsky, M. A. Bergmann, J. Buhler, S. Andersson, and V. Korenivski, Phys. Rev. B **86**, 214413 (2012).
[15] D. J. Chakrabarti, D. E. Laughlin, S. W. Chen, and Y. A. Chang, in *Phase Diagrams of Binary Copper Alloys*, edited by P. Subramanian, D. Chakrabarti, and D. Laughlin (ASM International, Materials Park, OH, 1994), pp. 276–286.
[16] C. G. Robbins, H. Claus, and P. A. Beck, Phys. Rev. Lett. **22**, 1307 (1969).
[17] T. J. Hicks, B. Rainford, J. S. Kouvel, G. G. Low, and J. B. Comly, Phys. Rev. Lett. **22**, 531 (1969).
[18] R. W. Houghton, M. P. Sarachik, and J. S. Kouvel, Phys. Rev. Lett. **25**, 238 (1970).
[19] G. Iannone, D. Zola, A. Angrisani Armenio, M. Polichetti, and C. Attanasio, Phys. Rev. B **75**, 064409 (2007).
[20] A. P. Thakoor and K. L. Chopra, J. Appl. Phys. **48**, 3850 (1977).
[21] I. Bakonyi, E. Tóth-Kádár, J. Tóth, T. Becsei, T. Tarnóczi, and P. Kamasa, J. Phys.: Condens. Matter **11**, 963 (1999).
[22] A. Rusanov, R. Boogaard, M. Hesselberth, H. Sellier, and J. Aarts, Physica C **369**, 300 (2002).
[23] A. F. Kravets, A. N. Timoshevskii, B. Z. Yanchitsky, O. Yu. Salyuk, S. O. Yablonovskii, S. Andersson, and V. Korenivski, J. Magn. Magn. Mater. **324**, 2131 (2012).
[24] J. J. Hauser, Phys. Rev. **187**, 580 (1969).
[25] J. S. Moodera and R. Meservey, Phys. Rev. B **29**, 2943 (1984).
[26] Z. Q. Qiu, H. Tang, Y. W. Du, G. P. Stern, and J. C. Walker, J. Appl. Phys. **63**, 3657 (1988).
[27] N. García and A. Hernando, J. Magn. Magn. Mater. **99**, L12 (1991).
[28] I. Navarro, M. Ortuño, and A. Hernando, Phys. Rev. B **53**, 11656 (1996).
[29] M. G. Samant, J. Stöhr, S. S. P. Parkin, G. A. Held, B. D. Hermsmeier, F. Herman, M. van Schilfgaarde, L.-C. Duda, D. C. Mancini, N. Wassdahl, and R. Nakajima, Phys. Rev. Lett. **72**, 1112 (1994).
[30] P. Swaminathan, R. A. Rosenberg, G. K. Shenoy, J. S. Palmer, and J. H. Weaver, Appl. Phys. Lett. **91**, 202506 (2007).
[31] B. Dieny, V. S. Speriosu, S. S. P. Parkin, B. A. Gurney, D. R. Wilhoit, and D. Mauri, Phys. Rev. B **43**, 1297 (1991).
[32] B. Dieny, V. S. Speriosu, S. Metin, S. S. P. Parkin, B. A. Gurney, P. Baumgart, and D. R. Wilhoit, J. Appl. Phys. **69**, 4774 (1991).
[33] J. van Driel, F. R. de Boer, K.-M. H. Lenssen, and R. Coehoorn, J. Appl. Phys. **88**, 975 (2000).
[34] I. L. Prejbeanu, M. Kerekes, R. C. Sousa, H. Sibuet, O. Redon, B. Dieny, and J. P. Nozières, J. Phys.: Condens. Matter **19**, 165218 (2007).
[35] S. N. Okuno and K. Inomata, Phys. Rev. Lett. **70**, 1711 (1993).
[36] S. S. P. Parkin, C. Chappert, and F. Herman, Europhys. Lett. **24**, 71 (1993).
[37] J.-F. Bobo, L. Hennet, M. Piecuch, and J. Hubsch, J. Phys.: Condens. Matter **6**, 2689 (1994).
[38] R. Nakatani, K. Hoshino, H. Hoshiya, and Y. Sugita, J. Magn. Magn. Mater. **166**, 261 (1997).
[39] N. N. Lathiotakis, B. L. Györffy, E. Bruno, and B. Ginatempo, Phys. Rev. B **62**, 9005 (2000).
[40] J. L. Leal and M. H. Kryder, J. Appl. Phys. **79**, 2801 (1996).
[41] J. C. S. Kools, W. Kula, D. Mauri, and T. Lin, J. Appl. Phys. **85**, 4466 (1999).
[42] E. C. Stoner, Proc. R. Soc. London A **165**, 372 (1938).
[43] A. González and A. Hernando, Phys. Rev. B **65**, 094432 (2002).
[44] A. Hernando, I. Navarro, and P. Gorría, Phys. Rev. B **51**, 3281 (1995).
[45] M. J. Donahue and D. G. Porter, OOMMF User's Guide, Interagency Report NISTIR 6376, http://math.nist.gov/oommf
[46] R. F. L. Evans, W. J. Fan, P. Chureemart, T. A. Ostler, M. O. A. Ellis, and R. W. Chantrell, J. Phys.: Condens. Matter **26**, 103202 (2014).